Controls on the hydraulic geometry of alluvial channels: bank stability to gravitational failure, the critical-flow hypothesis, and conservation of mass and energy

Jon D. Pelletier

5   Department of Geosciences, The University of Arizona, 1040 East Fourth Street, Tucson, Arizona 85721–0077, U.S.A.

Correspondence to: Jon D. Pelletier (jdpellet@email.arizona.edu)

Abstract. The bankfull depths, widths, depth-averaged water velocities, and along-channel slopes of alluvial channels are approximately power-law functions of bankfull discharge across many orders of magnitude. What mechanisms give rise to these patterns is one of the central questions of fluvial geomorphology. Here it is proposed that the bankfull depths of alluvial

10   channels are partially controlled by the maximum heights of gravitationally stable channel banks, which depend on bank material cohesion and hence on clay content. The bankfull depths predicted by a bank-stability model correlate with observed bankfull depths estimated from the bends in the stage-discharge rating curves of 387 U.S. Geological Survey gaging stations in the Mississippi River Basin. It is further proposed that depth-averaged water velocities scale with bankfull depths as a result of a self-regulatory feedback among water flow, relative roughness, and channel-bed morphology that limits depth-averaged

15   water velocities to be within a relatively narrow range associated with Froude numbers that have a weak inverse relationship to bankfull discharge. Given these constraints on channel depths and water velocities, bankfull widths and along-channel slopes consistent with observations follow by conservation of mass and energy of water flow.

1 Introduction

The bankfull depths, h, widths, w, depth-averaged water velocities, v, and along-channel slopes, S, of alluvial channels exhibit

20   power-law relationships with bankfull discharge, Q:

$$h \propto Q^k, w \propto Q^b, v \propto Q^m, S \propto Q^z \qquad (1)$$

where $k \approx 0.4$, $b \approx 0.5$, $m \approx 0.1$, and $z \approx -0.4$ (Leopold and Maddock, 1953). Many studies have proposed a process-based understanding of these patterns (see reviews by Ferguson (1986) and Singh (2003)), but none has achieved widespread acceptance.

25   Schumm (1960) documented that alluvial channels with sand-rich bed and bank material tend to be wide and shallow, while alluvial channels with silt-and-clay-rich bed and bank material tend to be narrow and deep. Schumm's findings have led nearly all subsequent researchers to consider the resistance of bank material to fluvial erosion to be the key factor controlling alluvial channel width (e.g., Parker, 1979; Eaton and Millar, 2004; Dunne and Jerolmack, 2019). Bank retreat, however, is also driven by gravitational failure (ASCE, 1999), a process that limits bank heights to values that depend on bank material cohesion and

30   hence on clay content. The gravitational failure of channel banks may partially control bankfull depths via a self-regulatory mechanism in which channel incision and/or floodplain deposition cause an increase in bank height, triggering bank failure when a critical bank height, dependent on bank material cohesion, is exceeded (Andrews, 1982). Bank failure results in channel widening, which may reduce depth-averaged water velocities and therefore tend to increase water depths (to convey similar water discharges) back towards the maximum stable bank height. This paper demonstrates that bankfull depths predicted by a

35   bank-stability model correlate with observed bankfull depths estimated from the bends in the stage-discharge rating curves of 387 U.S. Geological Survey (U.S.G.S.) gaging stations in the Mississippi River Basin (MRB). This analysis supports the hypothesis that the gravitational failure of channel banks partially controls bankfull depths and complements the recent work of Dong et al. (2019) that documented a relationship between bank-material texture and the hydraulic geometry of alluvial channels in the Selenga River Delta.

40   Grant (2000) proposed a critical-flow hypothesis in which depth-averaged water velocities are self-regulated via interactions among water flow, relative roughness, and channel-bed morphology. Grant (2000) argued that, for gravel-bedded channels above a threshold Froude number close to 1, much of the gravitational potential energy that would otherwise result in increased water velocities is lost to wave drag, especially that associated with flow around bed sediment grains protruding above the water surface (Wohl, 2013). For sand-bedded channels at Froude numbers typically in the range of 0.1-1, a similar increase in

45   drag occurs due to the formation of ripples and/or dunes that tend to develop in that range of Froude numbers (Simons and Richardson, 1966). These additional energy-loss mechanisms associated with critical or near-critical flow conditions, over and above the drag associated with subcritical flow over a smooth bed, can be expected to result in reduced depth-averaged water velocities and hence an increase in flow depths, resulting in lower Froude numbers and reduced relative roughness that, in turn, tend to increase in water velocities back towards a critical or near-critical state. Here it is proposed that the critical-flow

50   hypothesis constrains Froude numbers and hence the ratio of depth-averaged water velocities to the square root of bankfull depths to be within a relatively narrow range that has a weak inverse relationship to bankfull discharge.

    The bankfull widths of alluvial channels are set by the requirement that channels convey geomorphically effective water discharges. Conservation of mass, together with the clay-content control of bankfull depths and the Froude-number control of water velocities, thus constrains bankfull widths.

55   Conservation of energy constrains along-channel slopes. The conversion of gravitational potential energy into the kinetic energy of water leads to a relationship among along-channel slopes, bankfull Froude numbers, bankfull depths, and the size of the largest bed roughness elements, which in gravel-bedded channels tend to be bed sediment grains and in sand-bedded channels tend to be ripples and/or dunes.

2 Methods

60   ### 2.1 Controls on bankfull depths

The maximum stable height, h_c, of an alluvial channel bank subject to gravitational shear failure is (Chen et al., 1971; ASCE, 1999):

$$h_c = \frac{N_s}{\rho g} C, \tag{2}$$

where N_s is a stability parameter dependent on the angles of the bank and of internal friction, ρ is the bulk density of the bank material, g is the acceleration due to gravity, and C is the bank material cohesion (see Table 1 for a list of variables).

Bank material cohesion varies approximately linearly from 0 (for cohesionless sand) to 100 kPa (for pure clay) for moisture contents in the range of 7 to 40% (Fig. S1). Adopting a bulk density of 1700 kg m^{-3} and $N_s \approx 6$ (corresponding to a range of angles of the bank and of internal friction, including a vertical bank with an angle of internal friction of 25° (Table 1 of Chen et al., 1971)) results in an approximately linear relationship between the maximum stable bank height and the percent clay content, p_c, of the bank material (i.e., the floodplain deposits adjacent to the channel) with a proportionality coefficient of 0.35 (e.g., $h_c \approx 35$ m for pure clay bank material):

$$h_c \approx 0.35 p_c. \tag{3}$$

The model of this paper posits that bankfull depth is approximately equal to the maximum gravitationally stable bank height. With that assumption, Eq. (3) becomes

$$h \approx 0.35 p_c. \tag{4}$$

To test Eq. (4), the bankfull depths for 387 U.S.G.S. gaging stations in the MRB were estimated using the bends in the stage-discharge rating curves (Fig. S2). Predictions of bankfull depth using Eq. (4) were then compared to the observed bankfull depths derived from the rating curves. The gNATSGO soil database (Soil Survey Staff, 2019) was used to estimate the percent clay content of the floodplain deposits adjacent to each station. This analysis focuses on the MRB because there is no readily available soils database for any other continental-scale river basin that resolves floodplains in comparable detail and is based on a similar richness of field-based soil texture measurements.

The bankfull depth for each U.S.G.S. gaging station was estimated using the intersection of the linear regressions of peak annual gage height (used as a proxy for stage) to peak annual discharge obtained using the five smallest and five largest discharges in each record (shown as gray circles in the example of Fig. S2). This intersection, or bend, in the stage-discharge rating curve can identify the stage and discharge above which overbank flow occurs (Copeland et al., 2000), provided that the slope of the high-flow linear regression is much smaller than the slope of the low-flow linear regression. The analysis of this paper began by including data from all U.S.G.S. gaging stations in the MRB with available peak discharge data (U.S. Geological Survey, 2020). In order to maximize the accuracy of the analysis, however, only those stations that met the following criteria were retained: 1) at least 20 years of data, 2) a contributing area larger than 100 km^2, 3) at least a factor of five decrease in the slope of the stage-discharge rating curve from low flows to high flows, 4) a low-flow linear regression that extrapolates to a flow stage that has an absolute value within 50% of the bankfull depth at zero discharge, and 5) a resulting bankfull depth greater than 2 m. A total of 387 stations met these criteria. Stations for which the low-flow regression does not extrapolate to a flow stage close, i.e., within 50% of the bankfull depth, to zero at zero discharge may indicate that the gage

height is not an accurate proxy for flow stage and/or that data quality issues or river management practices preclude an accurate

95   estimate of bankfull depth using the stage-discharge rating curve.

To estimate the floodplain clay content for each of the 387 U.S.G.S. gaging stations, the depth-averaged percent clay content from soil depths of 5 to 150 cm was computed for every pixel within the MRB using gNATSGO. These depths were chosen to avoid the soil horizon close the surface (typically the O and/or A horizon, which can have clay contents reflective of surficial biological processes that are not representative of the rest of the profile) and because soil properties at depths greater than 150

100   cm can be inconsistently encoded in U.S. soil databases (Miller and White, 1998). A moving geometric mean (averaging distance of 10 km) of percent clay content was computed within floodplains mapped by Nardi et al. (2019). Because some U.S.G.S. gaging stations are located in channels with narrow floodplains that are not resolved in Nardi et al. (2019), the Nardi et al. (2019) floodplain map was augmented with single-pixel-width valleys defined by pixels with contributing areas larger than 100 km^2 following a steepest-descent routing of contributing area within the National Map Digital Elevation Model

105   (DEM) (Archuleta et al., 2017). Bankfull depths predicted by Eq. (4) were then compared to observed bankfull depths using a Pearson correlation coefficient, a root-mean-squared error (RMSE), the percentage of values correctly predicted to within a factor of 2, and a p-value that quantifies the likelihood of the null hypothesis that the predicted and observed bankfull depths may be correlated by chance.

To assess the impact of errors in percent clay content on predictions of the maximum stable bank height and therefore of

110   bankfull depth using Eq. (4), synthetic predictions for bankfull depths, $h_{\mathrm{pred,syn}}$, were generated equal to 0.35 times samples of synthetic percent clay content, $p_{\mathrm{c,syn}}$, drawn from a lognormal distribution designed to mimic the distribution of bankfull depths of U.S.G.S. gaging stations in the MRB, plus a normally distributed random error with a mean of zero and standard deviation of σ:

$$h_{\mathrm{pred,syn}} = 0.35\left(p_{\mathrm{c,syn}} + \sigma\eta\right) \tag{5}$$

115   where η is a normally distributed random variable with a mean of zero and a standard deviation of 1. For σ = 0, Eq. (5) produces synthetic data precisely equal to Eq. (4). With finite values of σ, Eq. (5) produces synthetic data with scatter that can be used to assess how errors in percent clay content may affect the relationships between observed and predicted bankfull depths.

2.2 Controls on depth-averaged water velocities and bankfull widths

120   The critical-flow hypothesis implies that bankfull Froude numbers, F, are limited to a relatively narrow range of values with an upper limit close to 1 for gravel-bedded channels and a similarly narrow but somewhat lower range of values for sand-bedded channels. In Sect. 3.2 it is demonstrated that this variation in F can be quantified using a power-law relationship between F and Q:

$$F \propto Q^n. \tag{6}$$

The power-law exponents reported in this paper were determined via a least-squares linear regression of the logarithms of the data. The definition of Froude number provides a linkage among depth-averaged bankfull water velocities, bankfull Froude numbers, and bankfull depths:

$$v = F\sqrt{gh}. \tag{7}$$

Equations (6) and (7) thus constrain the value of m to be

$$m = \frac{k}{2} + n. \tag{8}$$

The exponent b in the relationship between bankfull width and discharge can be constrained by conservation of mass of water assuming steady, uniform flow, consistent with many previous models for the downstream hydraulic geometry of alluvial channels (e.g., Lindley, 1919; Smith, 1974; Ferguson, 1986; Huang et al., 2004; Julien, 2014):

$$b = 1 - k - m. \tag{9}$$

2.3 Controls on along-channel slopes

The Darcy-Weisbach equation

$$v = \sqrt{\frac{8ghS}{f}}, \tag{10}$$

is based on conservation of energy for steady, uniform flow, i.e., that the gravitational potential energy per unit mass, ghS, produces a depth-averaged water velocity associated with a drag force per unit mass exerted by the channel bed on the water equal to $(f/8)v^2$, where f is the friction factor (e.g., Ferguson, 1986). Equation (10) can be rewritten as

$$S = \frac{F^2}{8}f. \tag{11}$$

Here the Variable Power Equation (VPE) of Ferguson (2007) is used to quantify f:

$$(8/f)^{1/2} = a_1 a_2 \beta^{-1} / \left(a_1^2 + a_2^2 \beta^{-5/3}\right)^{1/2} \tag{12}$$

where a_1 and a_2 are coefficients (equal to 6.1 and 2.4 based on the least-squares minimum error for velocity in the calibration performed by Ferguson (2007)), and β is the relative roughness. The VPE equation was chosen because it provides a transition between the Manning-Strickler $1/3^{rd}$ power scaling of friction factor to relative roughness for $\beta \gg 1$ (nearly all sand-bedded channels and some gravel-bedded channels) to a quadratic scaling when β is $\lesssim 1$ (channels with very coarse beds) that accords well with available data (Ferguson, 2007).

Relative roughness depends on whether or not bedforms are present. Table S2 of Ohata et al. (2019) identifies the range of F and d_{50} values conducive to ripple and/or dune development in alluvial channels. By cross-referencing those results with the Dunne and Jerolmack (D&J) (2018) global dataset, Sect. 3.3 demonstrates that 96% of sand-bedded channels in the D&J global dataset have F and d_{50} values conducive to ripple and/or dune development and therefore have a roughness that is likely dominated by bedforms rather than by bed sediment grains. The D&J global dataset includes 789 observations of d_{50}, S, and, h, and 711 observations of d_{50}, S, w, h, and Q drawn from the literature.

For gravel-(and-coarser)-bedded channels, relative roughness is defined in the calibration of Ferguson (2007) as the ratio of 84th percentile of bed grain diameter to the hydraulic radius. Since the analysis of this paper relates Eq. (12) to data from the D&J global dataset that uses d_{50} instead than d_{84}, it is assumed that $d_{50} \approx d_{84}/2$ and, because $w > 10h$ for all points in the D&J global dataset, that the bankfull hydraulic radius is approximately equal to the bankfull depth. The relative roughness for gravel-bedded channels, β_g, in the D&J global dataset can, therefore, be approximated as

$$\beta_g \approx \frac{2d_{50}}{h}. \tag{13}$$

For sand-bedded channels, relative roughness can by estimated as (Bathurst, 1993):

$$\beta_s \approx \frac{1.1H(1-e^{-25\alpha})}{3h} . \tag{14}$$

where H is the bedform height and α is the ratio of bedform height to length, L.

Combining Eqs. (11)-(14) gives an equation for the along-channel slopes of gravel-bedded channels consistent with conservation of energy:

$$S_g = \frac{F^2}{a_1^2 a_2^2}\left(\frac{2d_{50}}{h}\right)^2\left(a_1^2 + a_2^2\left(\frac{h}{2d_{50}}\right)^{5/3}\right), \tag{15}$$

and an analogous equation for sand-bedded channels:

$$S_s = \frac{F^2}{a_1^2 a_2^2}\left(\frac{1.1H(1-e^{-25\alpha})}{3h}\right)^2\left(a_1^2 + a_2^2\left(\frac{3h}{1.1H(1-e^{-25\alpha})}\right)^{5/3}\right). \tag{16}$$

The heights and lengths of ripples and dunes can be estimated as (Yalin, 1964):

$$H \approx \frac{h}{6}\left(1 - \frac{\tau_c}{\tau_0}\right), \tag{17}$$

and

$$L \approx 1000d_{50}. \tag{18}$$

Equation (16), therefore, can be rewritten in terms of d_{50}/h for a prescribed value of α as

$$S_s \approx \frac{F^2}{a_1^2 a_2^2}\left(\frac{18000\alpha(1-e^{-25\alpha})}{1.1\left(1-\frac{\tau_c}{\tau_0}\right)^2}\frac{d_{50}}{h}\right)^2\left(a_1^2 + a_2^2\left(\frac{1.1\left(1-\frac{\tau_c}{\tau_0}\right)^2}{18000\alpha(1-e^{-25\alpha})}\frac{h}{d_{50}}\right)^{5/3}\right). \tag{19}$$

3 Results

3.1 Controls on bankfull depths

Figure 1 illustrates the tendency for the clay contents of floodplain deposits adjacent to many smaller channels in the MRB to be lower than those of larger channels. For example, the North and South Platte Rivers have typical floodplain clay contents <10%, while the Platte River has typical floodplain clay contents of ≈10-20%, and the Missouri and Lower Mississippi Rivers have typical clay contents of ≈20-30%. There are many relatively small channels, however, that have clay contents > 30% due

to clay-rich local bedrock. As such, there isn't a precise, one-to-one correlation between clay content and contributing area or discharge, but rather a general tendency for channels conveying larger discharges to have more clay-rich floodplain deposits.
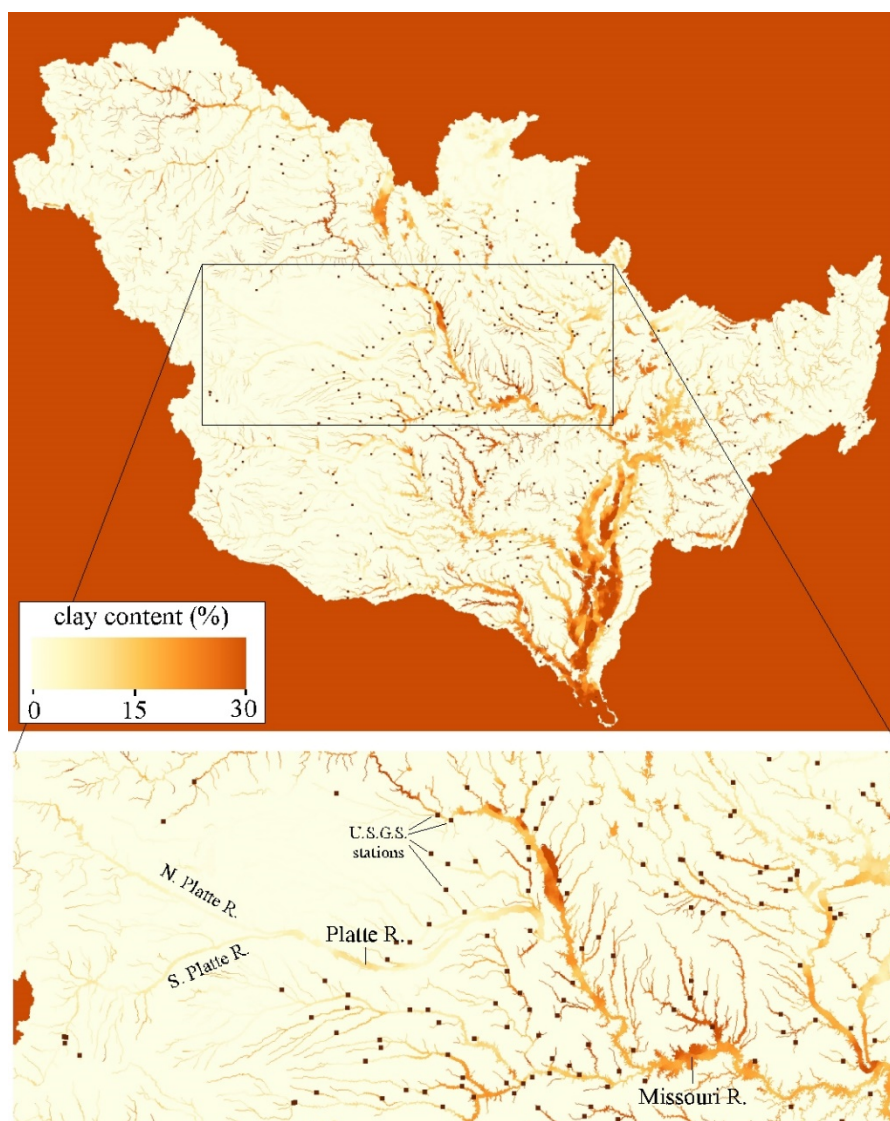
185

Figure 1: Color map of the average floodplain deposit clay content in the Mississippi River Basin. Also shown are the locations of the 387 U.S.G.S. gaging stations where predicted bankfull depths were computed using Eq. (4) and the observed bankfull depths were estimated based on the bends in the stage-discharge rating curves.

Figure 2(a) compares the bankfull depths predicted by Eq. (4) to observed bankfull depths estimated from the bends in the

190 stage-discharge rating curves. Predicted bankfull depths have a Pearson correlation coefficient of 0.42 with observed bankfull depths, a RMSE of 1.7 m, and 84% of the data points are within a factor of 2 of the observed bankfull depth. The p value, i.e., the chance that the correlation between h_{pred} and h_{obs} could have occurred by mere chance, is ~10^{-17}.

Earth **Surface**
Dynamics
Discussions

EGU

Figures 2(b) and 2(c) illustrate the potential impact of errors in percent clay contents on predicted bankfull depths using Eq. (5) with $\sigma = 0.06$ and 0.12 (6 and 12%), respectively. These σ values were chosen because, while gNATSGO does not provide

195 an error estimate, a recent soil property dataset created using machine learning algorithms has an estimated RMSE of 12% (Ramcharan et al., 2018) and a value half that size allows for the effect of error size to be assessed. For a relatively small error ($\sigma = 6\%$), there is a spread of values around the 1:1 line, with a larger relative spread for smaller clay contents, i.e., a 6% error results in a 100% relative error for a percent clay content of 6% (i.e., $h_{\mathrm{pred,syn}} \approx 2$ m) but a 50% relative error for a percent clay content of 12% (i.e., $h_{\mathrm{pred,syn}} \approx 4$ m). As the σ value increases to 12%, the spread of values around the 1:1 line increases as

200 expected but $h_{\mathrm{pred,syn}}$ values less than a few meters also appear to be biased upward (i.e., the geometric mean of $h_{\mathrm{pred,syn}}$ values deviate from the 1:1 line). This bias may be a result of percent clay content being bounded at zero, thus retaining the spread of values on the high side of the expected value only. Systematic deviations of h_{pred} from h_{obs} at low clay contents (i.e., percent clay contents $\lesssim 10\%$ and predicted bankfull depths $\lesssim 3$ m) may, therefore, be due to biases associated with the difficulty of measuring low clay contents with high relative precision. It is for this reason that stations with observed bankfull depths less

205 than 2 m were not retained in the analysis (Sect. 2.1).
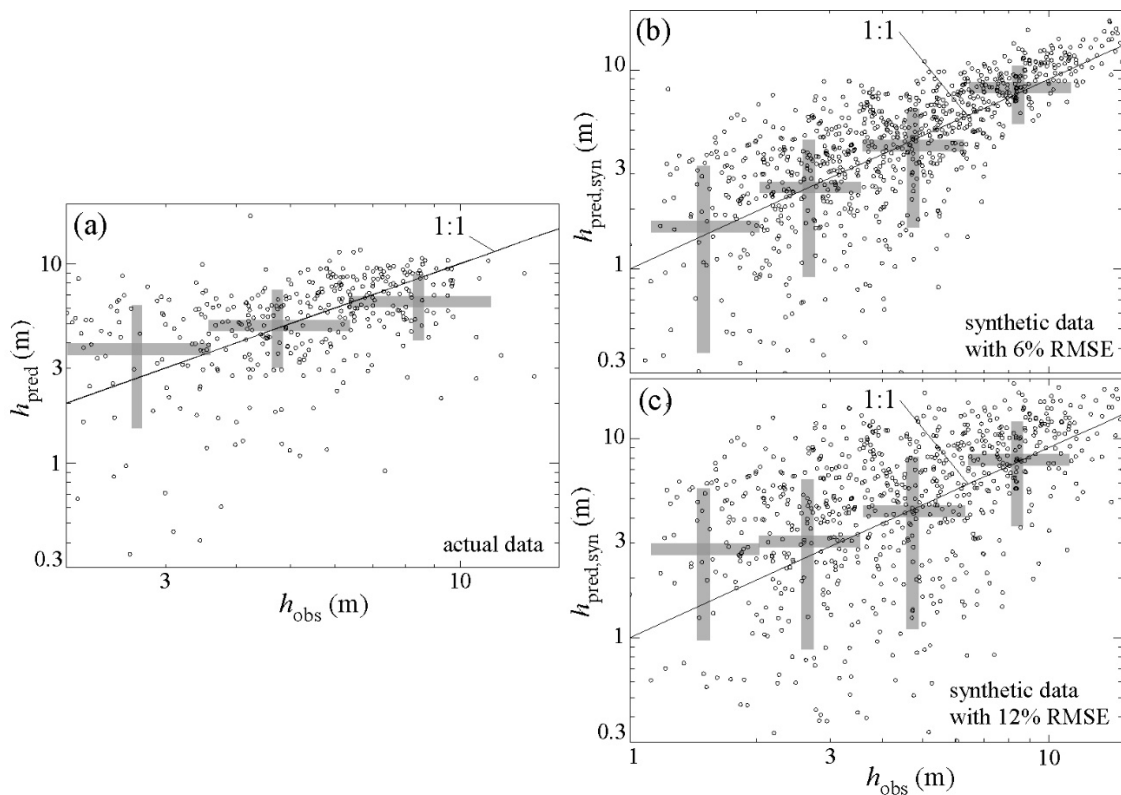
Figure 2: Plots of predicted bankfull depths, h_{pred}, calculated using Eq. (4) versus observed bankfull depths, h_{obs}, estimated based on the bends in the stage-discharge rating curves. (a) Actual data. (b)&(c) Synthetic data (Eq. (5)) with (b) $\sigma = 6\%$ and (c) $\sigma = 12\%$, respectively. The small open circles are individual data points and the gray rectangles illustrate the geometric means and standard
210 **deviations within each logarithmically spaced bin. The gray rectangles are for visualization purposes only – no analyses are performed on these values.**

Earth **Surface**
Dynamics
Discussions

3.2 Controls on depth-averaged water velocities and bankfull widths

Ripples and dunes tend to form at lower Froude numbers in channels with finer bed sediments (Fig. S3). The curve in Fig. S3

215   used to identify the range of F and d_{50} conditions conducive to ripple and/or dune development is reproduced in Fig. 3, where

96% of sand-bedded channels in the D&J global dataset are below the upper limits of F and d_{50} conducive to ripple and/or

dune development identified using the Ohata et al. (2019) dataset. As such, it is assumed for the purposes of this analysis that

sand-bedded channels in the D&J global dataset are dominated by bedform roughness while gravel-bedded channels in the

D&J global dataset are dominated by grain roughness.

220
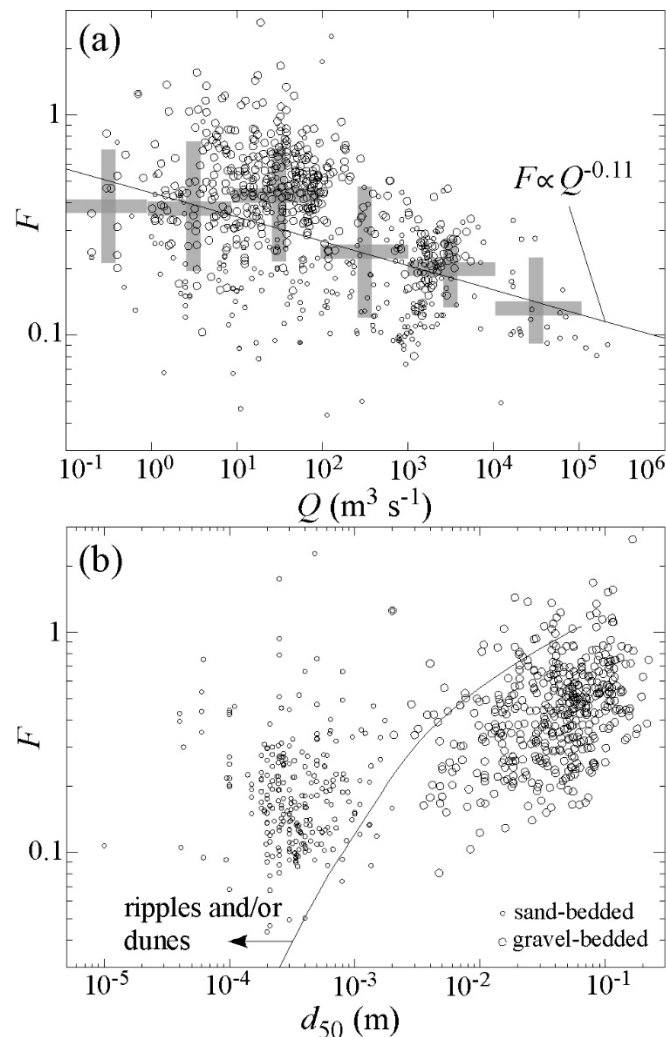
Figure 3: Bankfull Froude number relationships with bankfull discharge and median bed grain diameter. Plot of bankfull Froude number, F, as a function of (a) bankfull discharge, Q, and (b) median grain size, d_{50}, for the Dunne and Jerolmack (2018) global dataset. Small circles correspond to sand-bedded channels (d_{50} < 2 mm), large circles correspond to gravel-bedded channels (d_{50} > 2 mm). The curve in (b) defining channels that likely have ripples and/or dunes is based on the subset of 3791 field studies and

225   **experiments compiled by Ohata et al. (2019) and graphed in Fig. S3.**

Earth **Surface**
Dynamics
Discussions

Using the D&J global dataset, alluvial channel depths and widths scale with bankfull discharges to the 0.402 ± 0.006 and 0.512 ± 0.007 powers, respectively ($R^2 = 0.86$ and 0.89) (Fig. 4). If we take the -0.116 ± 0.009 Froude-number-discharge scaling exponent obtained from least-squares regression to the logarithms of the data (Fig. 3(a)) and the 0.402 ± 0.006 depth-

230   discharge scaling exponent as a starting point, Eqs. (8) and (9) predict a width-discharge exponent of 0.51 ± 0.01, i.e., precisely equal to that observed in the D&J global dataset.
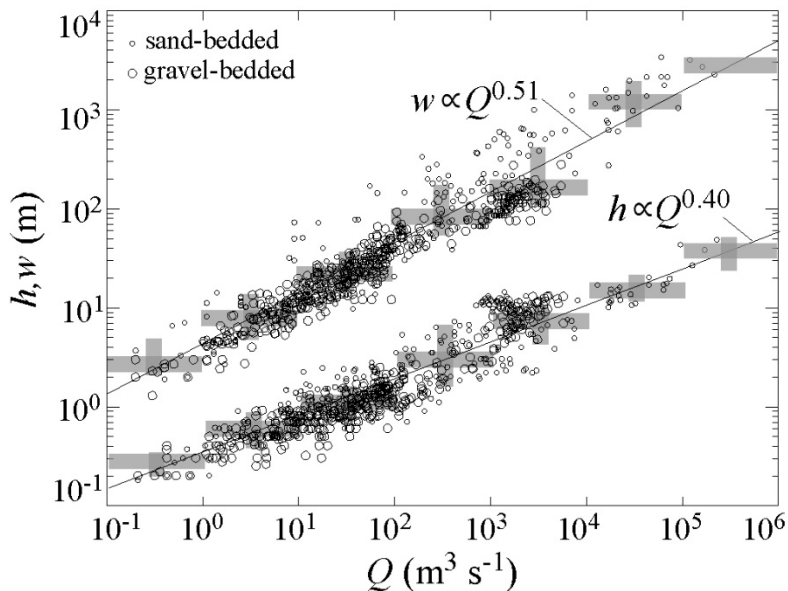
Figure 4: Plots of bankfull depth, *h*, and width, *w*, as a function of bankfull discharge, *Q*, from the Dunne and Jerolmack (2018)
235   **global dataset, along with least-squared linear regressions of the logarithms of the data, indicating *b* = 0.512 ± 0.007 and *k* = 0.402 ±**
0.006 for this dataset.

3.3 Controls on along-channel slopes

Along-channel slopes predicted by Eqs. (15) and (19) are consistent with observed values in the D&J global dataset (Pearson correlation coefficient of 0.77) (Fig. 5). For sand-bedded channels, in which ripples and/or dunes are likely to be the dominant

240   roughness elements, the predicted values plotted in Fig. 5 assume $\tau_c/\tau_0 \approx 0$ (consistent with the suspended-load-dominated conditions common in sand-bedded channels (Dade and Friend, 2000)) and a representative α value of 0.05 (based on the range 0.05-0.1 reported by Guy et al. (1966)). Figure S4 illustrates the sensitivity of the predictions of the along-channel slopes of sand-bedded channels to the presence/absence of bedforms and the assumed value of α. For alternative scenarios in which a) an unrealistically large value $\alpha = 0.25$ is assumed, and b) bed grains are assumed to be the dominant roughness elements (i.e.,

245   no bedforms are present), Eqs. (15) and (19) predict along-channel slopes that are approximately an order of magnitude above and below observed values, respectively.

Earth **Surface**
Dynamics
Discussions
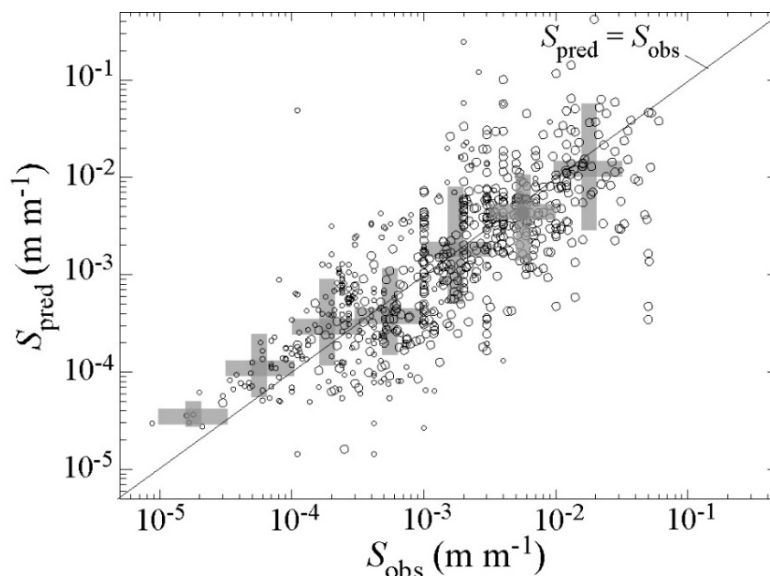
Figure 5: Plot of predicted along-channel slope, S_{pred}, using Eqs. (15) and (19) as a function of observed along-channel slope, S_{obs}, in the Dunne and Jerolmack (2018) global dataset. Predicted values for sand-bedded channels assume $\tau_c/\tau_0 \approx 0$ (consistent with the suspended-load-dominated conditions common in sand-bedded channels (Dade and Friend, 2000)) and $\alpha \approx 0.05$ (Guy et al., 1966).

4 Discussion

The model of this paper posits that floodplain deposit clay contents partially control the maximum stable heights of channel banks, but this control is not likely to result in a precise correlation between clay contents and bankfull channel depths for at least two reasons besides data errors. First, the incised depth of a channel that flows through a section of higher clay content to a section of lower clay content may be more strongly controlled by the lower clay content because the downstream reach may act as the local base level of erosion for the upstream reach. Second, alluvial channels can adjust to spatial variations in bank material cohesion by varying the bank angle in addition to the bank height (Knighton, 1974). For a 35° angle of internal friction, for example, a bank angle of 45° has a stability factor, N_s, that is approximately ten times larger than a vertical bank with the same cohesion (e.g., Fig. 3 of Chen et al., 1971). As such, an alluvial channel that flows through a section with less cohesive bank material compared to neighboring reaches may adopt a less steep bank (thus increasing the stability factor, N_s) instead of, or in addition to, becoming wider and shallower in order to minimize variations in channel depth that might otherwise drive large spatial variations in rates of aggradation/incision. Further tests of the model of this paper may require a better understanding of how channel depths adjust to spatial variations in bank material cohesion through a channel network.

It is also important to consider how potential errors in the data may contribute to the observed scatter in Fig. 2. The estimates of bankfull depths presented here are not exact because gage height (the height of the water above a reference point) is used as a proxy for flow stage. Also, uncertainties in clay content of just 5-10% percent are capable of creating scatter comparable to that in Fig. 2. Despite such large potential errors and the bias they may introduce into predictions of bankfull depths, the

analysis presented here rules out the possibility that floodplain deposit clay contents and bankfull depths are related by chance (i.e., $p \sim 10^{-17}$) and it demonstrates that Eq. (4) predicts bankfull depths to within a factor of 2 of the observed bankfull depths

270   for 84% of the 387 stations included in the analysis.

      The model of this paper posits that bankfull depth may be self-regulated via a tendency for an increase in bank height caused by channel incision and/or floodplain deposition to trigger bank failure when a critical bank height, dependent on bank material cohesion, is exceeded. This proposed self-regulatory mechanism does not require that gravitational shear failure be the dominant mechanism of bank retreat at all times (e.g., such failure may be more prevalent during periods of active incision

275   following major climatic changes), but it does require that gravitational shear failure play an important role in bank retreat. Such a role is consistent with process-based studies of bank retreat, in which bank retreat by gravitational shear failure has been documented to occur frequently during the falling limbs of flood discharges when pore pressures tend to be highest (e.g., Casagli et al., 1999; Simon et al., 2000). An important role for shear failure in bank retreat is also consistent with Li et al.'s (2015) finding that bankfull depth correlates with fluid viscosity because viscosity controls the permeability of bank material

280   and hence pore pressures and therefore susceptibility to gravitational shear failure. Fluvial erosion of the bank toe is necessary to remove material slumped from the bank into the channel and likely plays an important role in driving bank retreat in channels with cantilevered banks (Pizzuto, 1994). However, if the bank is more than twice the height of the zone of scour, gravitational shear failure nevertheless will be the process by which the majority of material is removed from the bank (Tao et al., 2019). The model of this paper is simplified in at least two specific ways that bear mentioning: it does not account for tension cracks

285   that, if present, can lower the maximum stable height below that predicted by Eq. (2) (Darby and Thorne, 1994), nor does it account for the role of vegetation in bank stability, which can increase bank heights by at least a factor of two over values predicted using bank material texture alone (Huang and Nanson, 1998).

      Two additional assumptions of the model should be emphasized. First, the model assumes a maximally incised channel, i.e., a channel that has incised to the point of reaching the threshold of bank stability quantified by Eq. (2). Quaternary climatic

290   changes have driven cycles in which channel aggradation has been followed by a positive feedback of incision and channel narrowing (e.g., Bull, 1991) that have likely made many alluvial channels prone to an incised state. Such considerations, however, do not apply to some types of alluvial channels, e.g., small-scale channels formed in the laboratory and those in which sediment supply is not heavily influenced by climatic changes. Second, the model of this paper involves no explicit constraint on the width-to-depth ratio of alluvial channels despite the fact that such a constraint may play an important role in

295   some cases. An important concept in rill erosion is that unit stream power is maximized for a width-to-depth ratio of $\approx 0.5\text{-}3$, with the specific value dependent on the cross-sectional functional form (e.g., Moore and Burch, 1986). A similar concept may limit incision in channels with small width-to-depth ratios (Huang and Nanson, 2000), reducing the likelihood of channels with $w/h \lesssim 1$ and hence potentially limiting h to values smaller than that set by Eq. (2) for channels with small discharges. Such a control does not seem likely in the channels of the D&J global dataset (since $w/h \gtrsim 10$), but it may play an important

300   role in some types of channels and should be explicitly considered in future research.

More data on the relationship between bank cohesion and bank material texture is needed. This study used clay content as a predictive variable for cohesion in part because a transfer function is available between clay content and cohesion based on the work of Dafalla (2013). However, silt content also affects cohesion (Huang et al., 2006) and the findings of Schumm (1960) suggest that both the silt and clay content of bank material are relevant to understanding alluvial channel geometry. The specific
305   surface area of bank material may be a more accurate predictive variable for cohesion than either clay content or silt and clay content (weighted equally), as specific surface area includes both the silt and clay contents but weighs the presence of clays more heavily (Huang et al., 2006).

The analysis presented here used a power-law relationship to quantify the relationship between F and Q (Eq. (6)). However, a scaling break appears to exist in the D&J global dataset (Fig. 3(a)), with F values approximately constant for Q values less
310   than $\sim 10^2$ m^3 s^{-1} (i.e., discharges dominated by gravel-bedded channels). This break may be consistent with the critical-flow hypothesis, i.e., steep, predominantly gravel-bedded channels in the D&J global dataset may have F values predominantly in the range of 0.3-1, independent of channel size/discharge, because the general lack of ripples and dunes in gravel-bedded channels requires that the increase in drag near critical flow conditions be caused primarily by wave drag, while in sand-bedded channels the increase in drag near critical-flow conditions is likely to be caused by ripples and/or dunes that form at a range of
315   Froude numbers weakly dependent on bankfull discharge. It would be useful for future research to investigate the relationships among F, Q, bed texture, and the presence/absence of ripples and/or dunes to more fully test this hypothesis and its implications for potential breaks in scaling within Eq. (1).

The model of this paper implicitly includes the sediment-supply control on along-channel slope documented by Li et al. (2005), Pfeiffer et al. (2017) and Blom et al (2017). Drainage basins with higher rates of sediment supply erode faster, resulting
320   in coarser sediments being delivered to channels, all else being equal (Attal et al., 2015). Coarser sediments increase along-channel slopes because steeper slopes are necessary to achieve critical or near-critical water velocities in alluvial channels with coarser bed sediments (Eqs. (15)&(19)).

5 Conclusions

This paper proposed that the bankfull depths of alluvial channels may be partially controlled by the maximum heights of
325   gravitationally stable channel banks, which depend on bank material cohesion and hence on clay content. Bankfull depths predicted by a bank-stability model correlate with the observed bankfull depths estimated using the bends in the stage-discharge rating curves for 387 U.S.G.S. gaging stations in the Mississippi River Basin. It was proposed, following Grant (2000), that depth-averaged water velocities scale with bankfull depths as a result of a self-regulatory feedback among water flow, relative roughness, and channel-bed morphology that limits velocities to be within a relatively narrow range associated with Froude
330   numbers that have a weak inverse relationship to bankfull discharge. Given these constraints on channel depths and depth-averaged water velocities, bankfull widths and along-channel slopes consistent with observations follow from conservation of mass and energy of water flow. The model of this paper provides a novel process-based understanding of the hydraulic

geometry of alluvial channel networks. Section 4 identified research needs that would enable a more comprehensive test of the hypotheses and a better understanding of the bank-textural controls on the hydraulic geometry of alluvial channels more
335   generally.

Data Availability The Supplementary Material contains all of the data used in the paper not published elsewhere.

Competing interests The author declares that he has no competing interest.

Acknowledgements I wish to thank the UA geomorphology research group, especially Luke A. McGuire and Alexander B. Prescott, for careful reviews that led to a significantly improved manuscript.

340   **References**

Allen, J. R. L.: A review of the origin and character of recent alluvial sediments, Sedimentology, 5, 89–191, https://doi.org/10.1111/j.1365-3091.1965.tb01561.x, 1965.

Andrews, E. D.: Bank stability and channel width adjustment, East Fork River, Wyoming, Water Resources Research, 18(4), 1184–1192, https://doi.org/10.1029/WR018i004p01184, 1982.

345   Archuleta, C. M., Constance, E. W., Arundel, S. T., Lowe, A. J., Mantey, K. S., and Phillips, L. A.: The National Map seamless digital elevation model specifications, U.S. Geological Survey Techniques and Methods, 11, B9, https://doi.org/10.3133/tm11B9, 2017.

ASCE Task Committee on Hydraulics, Bank Mechanics, and Modeling of River Width Adjustment: River width adjustment. 1. Processes and mechanisms, Journal of Hydraulic Engineering, 124(9), 881–902, 1998.

350   Attal, M., Mudd, S. M., Hurst, M. D., Weinman, B., Yoo, K., and Naylor, M.: Impact of change in erosion rate and landscape steepness on hillslope and fluvial sediments grain size in the Feather River basin (Sierra Nevada, California), Earth Surf. Dynam., 3, 201–222, https://doi.org/10.5194/esurf-3-201-2015, 2015.

Bathurst, J. C.: Flow resistance through the channel network, in Beven, K., and Kirkby, M.J., eds., Channel Network Hydrology, Wiley, Chichester, U.K., 43–68, 1993.

355   Blom, A., Arkesteijn, L., Chavarrías, V., and Viparelli, E.: The equilibrium alluvial river under variable flow and its channel-forming discharge, Journal of Geophysical Research Earth Surface, 122, 1924–1948, doi:10.1002/2017JF004213, 2017.

Bull, W. B.: Geomorphic Responses to Climatic Change, Oxford University Press, 1991.

Casagli, N., Rinaldi, M., Gargini, A. and Curini, A.: Pore water pressure and streambank stability: results from a monitoring site on the Sieve River, Italy. Earth Surf. Process. Landforms, 24: 1095-1114. https://doi.org/10.1002/(SICI)1096-
360   9837(199911)24:12<1095::AID-ESP37>3.0.CO;2-F, 1999.

Chen, W. F., Giger, M. W., and Fang, H. Y.: On the limit analysis of stability of slopes, Soils and Foundations, 9(4), 23–32, https://doi.org/10.3208/sandf1960.9.4_23, 1969.

Copeland, R. R., Biedenharn, D. S., and Fischenich, J. C.: Channel-Forming Discharge, U.S. Army Corps of Engineers Technical Note ERDC/CHL CHETN-VIII-5, 2000.

365 Dade, W. B., and Friend, P. F.: Grain-size, sediment-transport regime, and channel slope in alluvial rivers, The Journal of Geology, 106(6), 661–676. https://doi.org/10.1086/516052, 1998.

Dafalla, M. A.: Effects of clay and moisture content on direct shear tests for clay-sand mixtures, Advances in Materials Science and Engineering, 562726, https://doi.org/10.1155/2013/562726, 2013.

Darby, S. E., and Thorne, C. R.: Prediction of tension crack location and riverbank erosion hazards along destabilized channels,
370 Earth Surface Processes and Landforms, 19(3), 233–245, https://doi.org/10.1002/esp.3290190304, 1994.

Dong, T. Y., Nittrouer, J. A., Czapiga, M. J., Ma, H., McElroy, B., Il'icheva, E., et al.: Roles of bank material in setting bankfull hydraulic geometry as informed by the Selenga River Delta, Russia. Water Resources Research, 5, https://doi.org/10.1029/2017WR021985, 2019.

Dunne, K. B. J., and Jerolmack, D. J.: Evidence of, and a proposed explanation for, bimodal transport states in alluvial rivers,
375 Earth Surface Dynamics, 6, 583–594, https://doi.org/10.5194/esurf-6-583-2018, 2018.

Dunne, K. B. J., and Jerolmack, D. J.: What sets the width of a river? EarthArXiv preprint, http://doi.org/10.31223/osf.io/pvqag, 2019.

Eaton, B. C., and Millar, R. G.: Optimal alluvial channel width under a bank stability constraint, Geomorphology, 62, 35–45, https://doi.org/10.1016/j.geomorph.2004.02.003, 2004.

380 Ferguson, R. I.: Flow resistance equations for gravel- and boulder-bed streams, Water Resources Research, 43, W05427, https://doi.org/10.1029/2006WR005422, 2007.

Ferguson, R. I.: Hydraulics and hydraulic geometry, Progress in Physical Geography, 10(1), 1–31, https://doi.org/10.1177/030913338601000101, 1986.

Grant, G. E.: Critical flow constrains flow hydraulics in mobile-bed streams: A new hypothesis, Water Resources Research,
385 33(2), 349–358, https://doi.org/10.1029/96WR03134, 1997.

Guy, H. P., Simons, D. B., and Richardson, E. V.: Summary of alluvial channel data from flume experiments, 1956–1961, U.S. Geological Survey Professional Paper, 462-I, 1–96, 1966.

Huang, H. Q., Chang, H. H., and Nanson, G. C.: Minimum energy as the general form of critical flow and maximum flow efficiency and for explaining variations in river channel pattern, Water Resources Research, 40, W04502,
390 https://doi.org/10.1029/2003WR002539, 2004.

Huang, H. Q. and Nanson, G. C.: Hydraulic geometry and maximum flow efficiency as products of the principle of least action. Earth Surface Processes and Landforms, 25, 1–16, https://doi.org/10.1002/(SICI)1096-9837(200001)25:1<1::AID-ESP68>3.0.CO;2-2, 2000.

Huang, H. Q., and Nanson, G. C.: The influence of bank strength on channel geometry: An integrated analysis of some observations, Earth Surface Processes and Landforms, 23, 865–876, https://doi.org/10.1002/(SICI)1096-9837(199810)23:10<865::AID-ESP903>3.0, 1998.

Huang, J., Hilldale, R. C., and Griemann, B. P.: Chapter 4: Cohesive Sediment Transport, in Erosion and Sedimentation Manual, U.S. Department of Interior Bureau of Reclamation, Denver, Colorado, 2006.

Knighton, A. D.: Variation in width-discharge relation and some implications for hydraulic geometry, Geological Society of America Bulletin, 85(7), 1069–1076. https://doi.org/10.1130/0016-7606(1974)85<1069:VIWRAS>2.0.CO;2, 1974.

Leopold, L B., and Maddock, T Jr.: The Hydraulic Geometry of Stream Channels and Some Physiographic Implications, U.S. Geological Survey Professional Paper 252, 1953.

Li, C., Czapiga, M. J., Eke, E. C., Viparelli, E., and Parker, G.: Variable Shields number model for river bankfull geometry: bankfull shear velocity is viscosity-dependent but grain size-independent, Journal of Hydraulic Research, 53(1), 36–48, http://dx.doi.org/10.1080/00221686.2014.939113, 2015.

Lindley, E. S.: Regime channels. Proceedings, Punjab Engineering Congress, 7, 63, 1919.

Miller, D. A. and White, R. A.: A Conterminous United States Multi-Layer Soil Characteristics Data Set for Regional Climate and Hydrology Modeling. Earth Interactions, 2, 2, https://doi.org/10.1175/1087-3562(1998)002<0001%3AACUSMS>2.3.CO%3B2, 1998.

Moore, I. D. and Burch, G. J.: Sediment transport capacity of sheet and rill flow: Application of unit stream power theory, Water Resources Research, 22(8), 1350–1360, https://doi.org/10.1029/WR022i008p01350, 1986.

Nardi, F., Annis, A., Di Baldassarre, G. et al.: GFPLAIN250m, a global high-resolution dataset of Earth's floodplains, Scientific Data, 6, 180309, https://doi.org/10.1038/sdata.2018.309, 2019.

Ohata, K., Naruse, H., Yokokawa, M., and Viparelli, E.: New bedform phase diagrams and discriminant functions for formative conditions of bedforms in open-channel flows, Journal of Geophysical Research Earth Surface, 122, 2139–2158. https://doi.org/10.1002/2017JF004290, 2017.

Parker, G.: Hydraulic geometry of active gravel rivers, Journal of the Hydraulics Division of the America Society of Civil Engineers, 105, 1185–1201, 1979.

Pfeiffer, A. M., Finnegan, N. J., and Willenbring, J. K.: Sediment supply controls equilibrium channel geometry in gravel rivers, Proceedings of the National Academy of Sciences of the U.S.A., 114(13), 3346–3351, https://doi.org/10.1073/pnas.1612907114, 2017.

Pizzuto, J.: Equilibrium bank geometry and the width of shallow sandbed streams, Earth Surface Processes and Landforms, 9, 199–207, 1994.

Ramcharan, A., Hengl, T., Nauman, T., Brungard, C., Waltman, S., Wills, S. and Thompson, J.: Soil Property and Class Maps of the Conterminous United States at 100-Meter Spatial Resolution, Soil Science Society of America Journal, 82: 186–201, https://doi.org/10.2136/sssaj2017.04.0122, 2018.

Schumm, S. A.: The shape of alluvial channels in relationship to sediment type, U.S. Geological Survey Professional Paper 352-B, 1960.

Simon, A., Curini, A., Darby, S. E., and Langendoen, E. J.: Bank and near-bank processes in an incised channel, Geomorphology, 35, 193–217, 2000.

Simons, D. B., and Richardson, E. V.: Resistance to Flow in Alluvial Channels, U.S. Geological Survey Professional Paper 422-J, U.S. Government Printing Office, Washington, D.C., 1966.

Singh, V. P.: On the theories of hydraulic geometry, International Journal of Sediment Research, 18(3), 196–218, 2003.

Smith, T. R.: A derivation of the hydraulic geometry of steady-state channels from conservation principles and sediment transport laws, The Journal of Geology, 82(1), 98–104, https://doi.org/10.1086/627939, 1974.

Soil Survey Staff. Gridded National Soil Survey Geographic (gNATSGO) Database for the Conterminous United States. United States Department of Agriculture, Natural Resources Conservation Service. Available online at https://nrcs.app.box.com/v/soils, 2019.

Tao, G., Chen, J., and Pan, Y.: An improved analysis model for cantilever failure of composite riverbanks and collapse simulation, IOP Conference Series, Earth and Environmental Science, 304, 032045, https://doi.org/10.1088/1755-1315/304/3/032045, 2019.

U.S. Geological Survey, Peak Streamflow for the Nation, Digital data available at https://nwis.waterdata.usgs.gov/usa/nwis/peak, 2020.

Wohl, E.: Mountain Rivers Revisited, John Wiley & Sons, New York, 2013.

Yalin, M. S.: Geometrical properties of sand wave, Journal of Hydraulic Division of the American Society of Civil Engineering, 90(HY5), 105–119, 1964.

Table 1: List of variables

Symbol	Variable Name/Description	Units	Reference value(s)
a_1	coefficient in VPE model		6.1
a_2	coefficient in VPE model		2.3
α	ratio of ripple or dune height to length		0.05
b	exponent in power-law scaling of bankfull width and discharge		0.51
β	roughness ratio		
β_g	roughness ratio for gravel-bedded channels		
β_s	roughness ratio for sand-bedded channels		
C	bank material cohesion	kPa	0-100
d_{50}	median bed grain diameter	mm	
η	normally distributed random variable		
f	friction factor		
F	bankfull Froude number		
g	acceleration due to gravity	m s^{-2}	9.81
h	bankfull channel depth	m	
h_{pred}	bankfull channel depth predicted by Eq. (4)	m	
$h_{pred,syn}$	synthetic bankfull channel depth predicted by Eq. (5)	m	
h_{obs}	observed bankfull channel depth	m	
h_c	maximum stable bank height	m	
H	bedform height		
k	exponent in the power-law relationship between bankfull depth and discharge		0.40
L	bedform spacing		
m	exponent in the power-law relationship between velocity and bankfull discharge		0.1
n	exponent in the power-law relationship between bankfull Froude number and bankfull discharge		-0.11
N_s	stability parameter in bank mass failure equation		6
p_c	percent clay content in bank material		
$p_{c,syn}$	synthetic percent clay content in bank material		
Q	bankfull discharge	m^3 s^{-1}	
ρ	bank material bulk density	kg m^{-3}	1700
S	along-channel slope		
σ	standard deviation of synthetic percent clay content		0.06, 0.12
τ_c	boundary shear stress threshold for entrainment	Pa	
τ_0	boundary shear stress	Pa	
v	depth-averaged water velocity	m s^{-1}	
w	bankfull channel width	m	
z	exponent in the power-law relationship between along-channel slope and bankfull discharge		-0.4

450